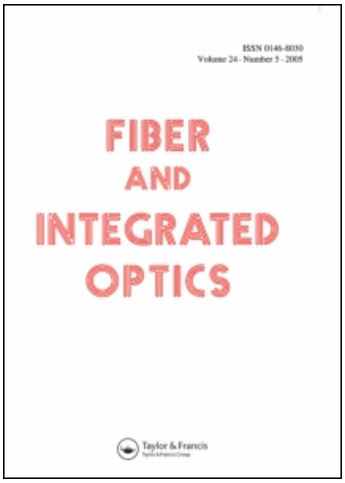

Fiber and Integrated Optics
Publication details, including instructions for authors and subscription information:
http://www.informaworld.com/smpp/title~content=t713771194

Fiber Bragg Grating Structures with Fused Tapers

S. F. O. Silva[a]; L. A. Ferreira[a]; F. M. Araújo[a]; J. L. Santos[ab]; O. Frazão[ab]
[a] INESC Porto, Porto, Portugal [b] Departamento de Física da Faculdade de Ciências, da Universidade do Porto, Porto, Portugal

Online publication date: 08 February 2011

To cite this Article Silva, S. F. O. , Ferreira, L. A. , Araújo, F. M. , Santos, J. L. and Frazão, O.(2011) 'Fiber Bragg Grating Structures with Fused Tapers', Fiber and Integrated Optics, 30: 1, 9 — 28
To link to this Article: DOI: 10.1080/01468030.2010.526287
URL: http://dx.doi.org/10.1080/01468030.2010.526287

Fiber and Integrated Optics, 30:9–28, 2011

ISSN: 0146-8030 print/1096-4681 online
DOI: 10.1080/01468030.2010.526287

Taylor & Francis
Taylor & Francis Group

Fiber Bragg Grating Structures with Fused Tapers

S. F. O. SILVA,[1] L. A. FERREIRA,[1] F. M. ARAÚJO,[1]
J. L. SANTOS,[1,2] and O. FRAZÃO[1,2]

[1]INESC Porto, Porto, Portugal
[2]Departamento de Física da Faculdade de Ciências da Universidade do Porto, Porto, Portugal

Abstract *Fiber structures based on the combination of abrupt tapers and fiber Bragg gratings are studied. Two situations are explored—in one, the taper is fabricated in the fiber region with a fiber Bragg grating; in the other, the taper is first fabricated followed by the fiber Bragg grating. It is shown that the first device presents the properties of a Fabry-Perot cavity and the other of a phase-shifted Bragg grating, where the phase shift is associated to the tapered fiber region. The sensing characteristics of these structures are studied, and it is shown that the temperature sensitivities are similar but with observable different responses to strain.*

Keywords fiber Bragg grating, optical fiber sensors, optical fiber tapers, strain and temperature measurement

1. Introduction

The single-mode fiber taper is a simple fiber structure and the basis of many optical fiber devices that are used in several contexts, such as interferometry [1], biosensors [2], and fiber dye lasers [3]. Tapered fiber devices rely on the interaction of the evanescent field surrounding the fiber waist with the external environment and, therefore, are an alternative to core-exposed fibers when the objective is to develop sensors. The shape of the taper is also of great importance in applications, where its deformation must be rigorously controlled, for example, in directional couplers [4, 5], in some sensors based on bending [6, 7], and in beam expanders [8].

Tapers in optical fibers have essentially been made in two ways: by etching the fiber cladding [9–11] or by lengthening the fiber by fusion [12–15]. Methods are based in a fusion range, from translating the fiber into a CO_2 laser beam [12], heading a fiber horizontally over a traveling gas burner [13], or by using a fusing-and-pulling treatment with a manual fiber fusion splicer [14, 15].

The combination of fiber Bragg gratings (FBGs) with tapers has been widely studied, and many tapered structures have been developed for sensing applications. Etched fibers have a uniform core and, thus, a constant propagation coefficient [16]. However, in tapers

Received 15 June 2010; accepted 20 September 2010.
Address correspondence to O. Frazão, INESC Porto, Rua do Campo Alegre 687, 4169-007 Porto, Portugal. E-mail: ofrazao@inescporto.pt

made by fusion, the fiber core is tapered as well; and therefore, they have non-uniform propagating properties capable of originating non-uniform gratings. In particular, the combination of two FBGs separated by an abrupt tapered region permit the formation of Fabry-Perot interferometers with novel properties. An example of this is a recently reported work, where it was shown how the strain sensitivity of FBGs can be controlled when used in combination with fused tapers [17].

This article presents the analysis of abruptly fused tapers fabricated over an FBG and the other way around, i.e., fabricating a Bragg grating in a tapered core fiber. Also studied are the properties of these structures for measurement of strain and temperature.

2. Fiber Tapers

Taper components have been modeled by assuming exponential, parabolic, sinusoidal, polynomial, or other taper profiles [18–21]. Here the assumed model is developed for a taper with an exponential profile [22]. Its fabrication relies on the fiber being placed under tension into a particular heat source; the length of the heated region is maintained constant as tapering proceeds, thus forming a taper. Therefore, the taper is a structure comprising a narrow stretched filament—the *taper waist*—between conical tapered sections—the *taper transition*—which are linked to the unstretched fiber. Figure 1a shows the general structure of an optical fiber taper.

Optically, at the beginning of the taper, the fundamental mode propagates as a core mode. As the fundamental mode enters the taper transition section, assuming it is thin enough, it begins to spread out into the cladding region until the core-cladding waveguiding structure cannot support the mode. From this point, the mode enters the taper waist as a cladding mode. Here, the cladding and the surrounding medium act as the waveguiding structure. Intuitively, the most sensitive region is the taper waist, where the overall device diameter is at a minimum, and hence, the evanescent field intensity is most pronounced. The quantities used to describe the shape of a complete fiber taper are illustrated in Figure 1b.

In this simple model, it is assumed that a fixed length L_o of fiber is to be uniformly heated and stretched, whereas outside this *hot-zone*, the fiber is cold and solid [22]. The taper is formed symmetrically so that the two taper transitions are identical. The radius of the optical fiber without a taper is r_o, and the uniform taper waist has length L_w and radius r_w. Each identical taper transition has a length z_o and a shape described by a decreasing local radius function $r(z)$, where z is the longitudinal coordinate. The origin of z is at the beginning of each taper transition (points P and Q) and, following that notation, $r(0) = r_o$ and $r(z_o) = r_w$.

Here the simplest example of the *constant hot-zone* is followed [22], where $L_w = L_o$. Assuming that the fiber radius follows a decaying exponential profile in the taper sections, it can be written that

$$r(z) = r_o \exp\left[-\frac{z}{L_o}\right] \qquad (0 \le z \le z_o). \tag{1}$$

The shape of the abrupt tapers presented in this work is described by Eq. (1). They were fabricated by fusion, where an arc discharge was used while the fiber (SMF-28, Corning, USA) was placed under tension. Figure 1c shows a photo of one of these tapers with a $\sim$400 μm length. The ratio r_w/r_o is approximately 0.65 and corresponds to six arc discharges. The number of these discharges affects the taper diameter at the waist, as

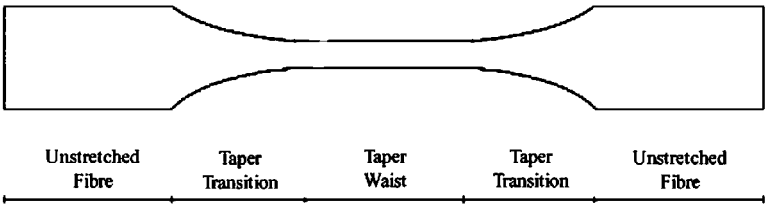

(a)

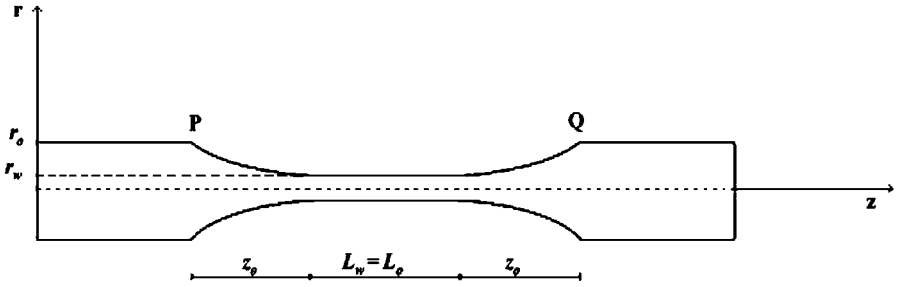

(b)

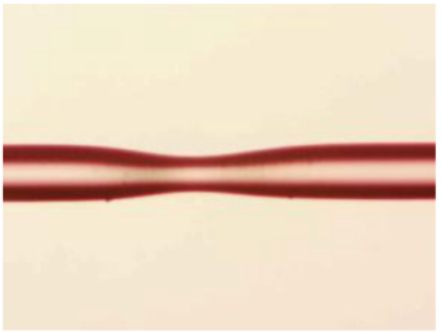

(c)

Figure 1. (a) Schematic of an optical fiber taper, (b) relevant design parameters, and (c) photo of a fabricated taper.

Figure 2a shows. Since the fiber is held under tension and is locally heated, the increase of arc discharges will decrease the strength of the fiber, leading rapidly to its break. However, this non-linear behavior will depend on the intensity of the arc, the alignment of the fiber, and the tension applied.

The losses introduced by the fabrication process are negligible, since the tapered fiber transitions approximately satisfy the adiabatic criteria [23]. Figure 2b shows the results obtained. One can observe that between the fourth and the seventh arc discharge, there is a decrease of optical loss. This might be due to the re-coupling of light from the external environment into the core. The last arc discharge originated the entire fusion between the cladding and the core of the fiber, thus forming a very narrow taper. Even for this case, the process loss did not exceed 2 dB.

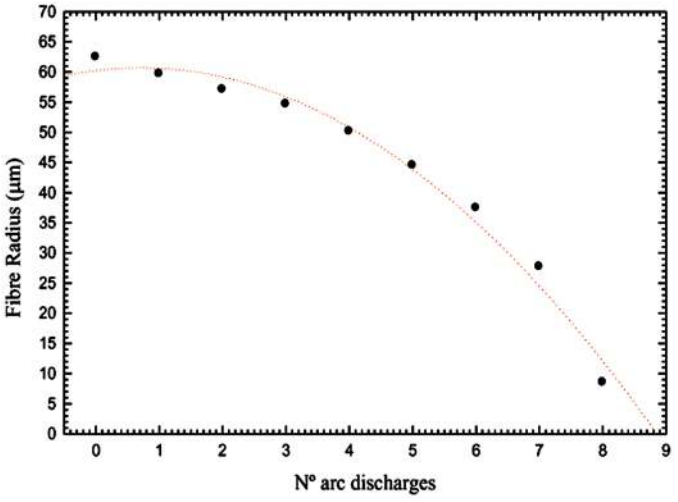

(a)

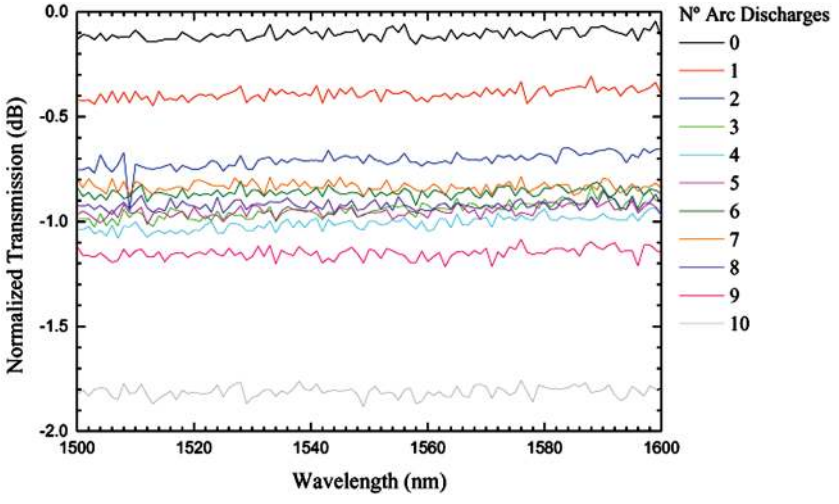

(b)

Figure 2. (a) Waist radius variation with number of arc discharges and (b) losses introduced in the taper fabrication process.

3. FBGs with Taper Structures

An optical fiber with a taper structure has non-uniform propagating properties due to the fiber geometry in that section but also due to the effective index variation. The fundamental propagation mode has a non-uniform effective index $n_{eff}(z)$, because the fiber radius decreases along the taper, and consequently, the grating has a variable Bragg wavelength. For small variations of the effective index along the fiber, the Bragg wavelength along the grating can be expressed in the following form:

$$\lambda_B(z) = \lambda_B(0)\left[1 + \frac{\Delta n_{eff}(z)}{n_{eff}(0)}\right], \tag{2}$$

where $\lambda_B(0)$ and $n_{eff}(0)$ are, respectively, the Bragg wavelength and the effective index at the beginning of the grating, i.e.,

$$\lambda_B(0) = 2\Lambda n_{eff}(0), \tag{3}$$

and $\Delta n_{eff}(z)$ is the index variation along the grating

$$\Delta n_{eff}(z) = n_{eff}(z) - n_{eff}(0). \tag{4}$$

Equation (2) can be written as

$$\lambda_B(z) = 2\Lambda n_{eff}(z). \tag{5}$$

The effective index of the core mode, $n_{eff}(z)$, is given as a function of the propagating wavelength, the geometry of the fiber, and the refractive index of the core material [24]. For a weakly guiding step-index fiber, a geometric-optics approximation is generally used to yield the effective indices of the core and the cladding modes [25]. Because a single-mode fiber can support only the LP_{01} mode, the equation for the core mode is

$$\frac{2\pi}{\lambda} D_{core}\left[(n_{core})^2 - (n_{eff})^2\right]^{1/2} - \frac{\pi}{2} = 2\cos^{-1}\left[\frac{(n_{core})^2 - (n_{eff})^2}{(n_{core})^2 - (n_{clad})^2}\right]^{1/2}, \tag{6}$$

where D_{core} is the diameter of the core, and n_{core} and n_{clad} are the refractive index of the core and cladding materials, respectively. This equation is solved numerically and gives the relation between the core radius and the effective index. Hence, using Eq. (5), the dependence of the Bragg wavelength with the core diameter can be determined.

It is relevant to emphasize that, as indicated in Section 1, there are many works that address the combination of tapers and FBGs. However, quite often the tapers extend over a substantial FBG length, resulting essentially in a structure with a chirped-FBG-like response. When abrupt tapers are considered, its small length compared with that of the grating originates a clear split of one grating in two (for the case of an abrupt taper over an FBG) or a grating with a refractive index modulation in its central region (when an FBG is written over an abrupt taper). As will be shown in what follows, in both cases, Fabry-Perot-like interference effects appear with specific behavior when strain and temperature are applied to these fiber structures.

Two optical fiber devices based on the combination of an abrupt taper and a single Bragg grating (TFBG) are now presented. In one, the taper is fabricated over an FBG ($TFBG_1$); while in the other, it is the taper that is fabricated first followed by the FBG ($TFBG_2$). In both cases, the electric arc technique was used to fabricate the tapers. The optical fiber was placed under tension, which allowed controlling the radius and length of each structure, while a translation stage was used for the precise positioning of the tapers. Also, FBGs were fabricated in series, in order to obtain sensing structures with similar spectral characteristics. FBGs were written with UV exposure through a phase mask (pitch of 1,044 nm) by using an excimer laser operating at 248 nm. The sensing structures were then interrogated by a tunable laser source, and the optical spectra is acquired by a LabView™-based program (National Instruments, USA) developed for this purpose.

To research the structure of $TFBG_1$, a Bragg grating was used with 10 mm length and written in a hydrogen-loaded single-mode fiber (SMF-28). At the middle of the grating, an abruptly fused taper was induced (six arc discharges, $\sim$400 μm length). For the $TFBG_2$

structure, a branch of single-mode fiber (SMF-28) was used, where an abruptly fused taper was fabricated (six arc discharges, $\sim$400 μm length). After being hydrogen loaded, a single Bragg grating was written in this optical fiber, noting that the abruptly fused taper should be at the center of the grating. The optical spectra of structures $TFBG_1$ and $TFBG_2$ are shown in Figures 3a and 3b, respectively.

The $TFBG_1$ structure indicates that the grating is essentially destroyed in the taper section, generating a true fiber Fabry-Pérot interferometer. The mirrors are the two unaffected lengths of the initial grating in each side of the taper section. Because these

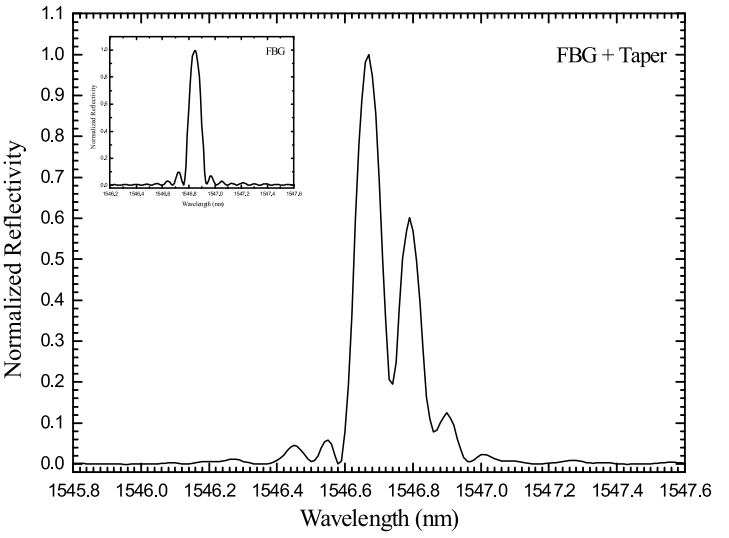

(a)

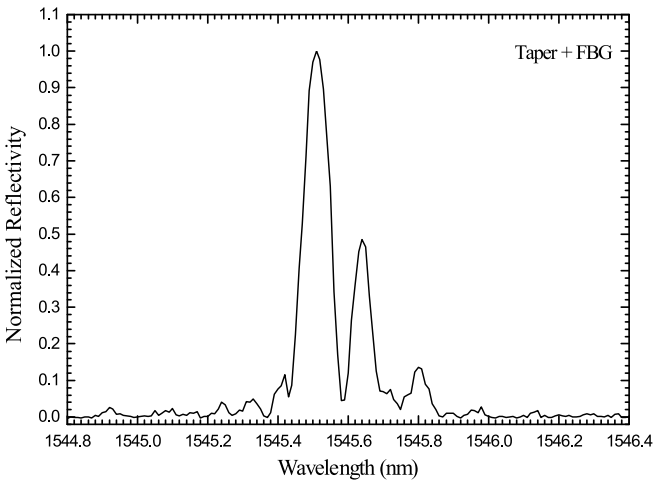

(b)

Figure 3. Optical spectra of an FBG: (a) with a short fused taper and (b) of a Bragg grating written in a tapered core fiber. The spectral reflectivity of the FGB alone is shown in the inset pictures.

lengths are smaller than the initial Bragg length, their spectral bandpass signatures are wider, which is confirmed by the experimental results.

Concerning the $TFBG_2$ structure, the fabrication of the abruptly fused taper changes not only the effective refractive index in the region, but also eliminates any residual photosensitivity that could exist in the fiber. However, after the fiber undergoes the hydrogen loading process, it is feasible afterward to write a Bragg grating in that region. The important difference, relative to the reverse-order sequence (grating written first and taper fabrication afterward), is that now there is a continuous grating, with a constant (in first order) refractive index amplitude modulation, on the top of an average refractive index value that changes in the device central region due to the previous taper fabrication operation. This progressive change introduces a progressive variation on the grating phase, resulting in a spectral signature typical of a phase-shifted Bragg grating structure. (It is important to notice that the length of the taper region, $\sim$400 μm, is much smaller than the grating length, $\sim$10 mm, which means the region of the phase variation can be viewed as a perturbation in the central region of the FBG). On the other hand, the control of the several fabrication parameters, as well as the FBGs spectral characteristics, will contribute significantly for the spectral response of the devices.

Therefore, these results indicate that fabricating an abruptly fused taper in an FBG ($TFBG_1$) or a Bragg grating in a tapered core fiber ($TFBG_2$) originates fiber structures that are conceptually different. $TFBG_1$ is a Fabry-Perot interferometer, because the arc discharge erases the grating in the taper section (in practice, the structure will be formed by two shorter Bragg gratings separated by a tapered cavity). In $TFBG_2$, the grating is written in the taper section where the effective index is different, thus causing a phase change, resulting in a phase-shifted FBG device.

4. Sensing Characteristics

In the previous section, it was shown that a Fabry-Pérot cavity can be created with an abruptly fused taper in the middle of an FBG (tapered Fabry-Perot structure [TFP], $TFBG_1$). Basically, this tapered structure will act as a two-wave interferometer formed by two shorter gratings, which are the distributed mirrors (Figure 4a). As reported elsewhere [26], the equivalent reflection of a uniform FBG with total length L_T appears at the middle of the structure, which corresponds, in this case, to the position of each mirror and, hence, where the two waves seem to be reflected. Assuming that each grating has length L_1 and the fused taper has length L_2, then the cavity length is given by $L = L_1 + L_2$. Inducing two abruptly fused tapers equally spaced in the FBG will split the grating into three shorter gratings, thus forming two concatenated Fabry-Perot cavities with the same length, as shown in Figure 4b. In the same way, inducing three abruptly fused tapers equally spaced in the FBG will split the grating into four shorter gratings, thus forming three concatenated Fabry-Pérot cavities with the same length (Figure 4c).

The tapers were fabricated using the electric arc technique. An optical fiber with an FBG was placed under tension, which allowed controlling the radius and length of each structure, while a translation stage was used for the precise positioning of the tapers in the FBG region. The initial grating had a length of $\sim$10 mm and the abrupt tapers a length of $\sim$400 μm.

To better evaluate the proposed model, these TFP structures were theoretically analyzed. Figure 5 shows the spectral reflectivity of the three structures obtained experimentally and the corresponding simulations.

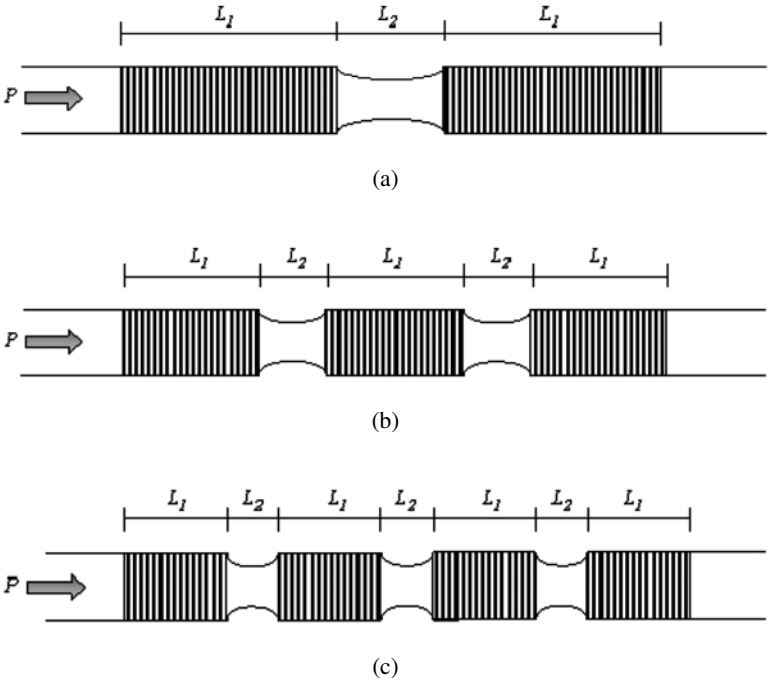

Figure 4. Schematic of FBG-based Fabry-Pérot interferometers: (a) single cavity, (b) two concatenated cavities, and (c) three concatenated cavities.

Fairly good agreement was observed between the experimental and simulated results. As expected, the precise control of the fabrication parameters, as well as increasing the complexity of the TFP structure, will contribute significantly to their spectral responses, as is shown in the simulations of the several TFP devices, in particular TFP_3 (Figure 5c).

A channeled spectrum in the reflection band is observed for each TFP, which becomes increasingly structured when the number of concatenated Fabry-Pérot sections increases. The periodicity of the fringes is 0.10 nm, 0.11 nm, and 0.12 nm for TFP_1, TFP_2, and TFP_3, respectively. The increase of the bandwidth envelope of each TFP is due to the presence of gratings with shorter lengths. The corresponding values are approximately 0.2 nm, 0.4 nm, and 0.6 nm. To better evaluate these results, the spectral behavior of the equivalent uniform Bragg gratings was performed, and the corresponding theoretical values obtained were 0.19 nm, 0.37 nm, and 0.55 nm. Notice that, in practice, the arc discharge during the fabrication process destroys the FBG in a region longer than the taper length. Theoretical analysis shows that, for a 400 μm-long taper, each affected region has a total length of 1.5 mm. Thus, for the experimental TFP structures, the length of the unaffected FBGs after the fabrication of tapers is smaller than the one predicted theoretically.

These TFP structures were submitted to strain and temperature. Concerning applied strain, the results obtained are shown in Figure 6, where the wavelength evolution of the three peaks identified in Figure 5 is presented.

The peaks wavelength shifts are associated with the channeled spectrum and, therefore, with the interferometric transfer function of the structure. As Table 1 shows, there

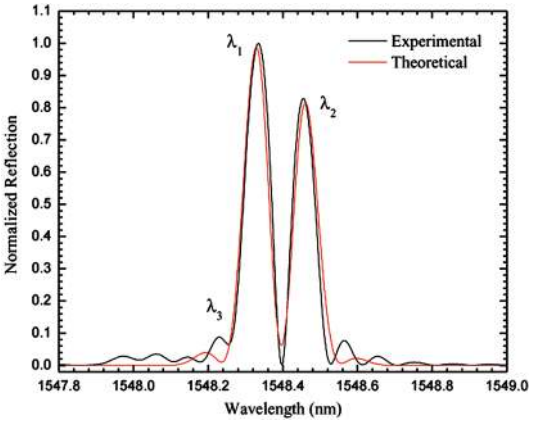

(a)

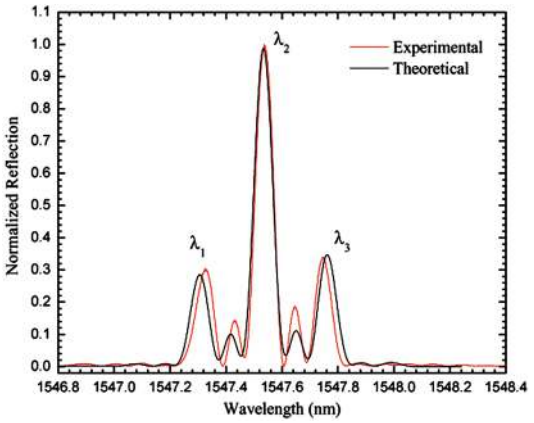

(b)

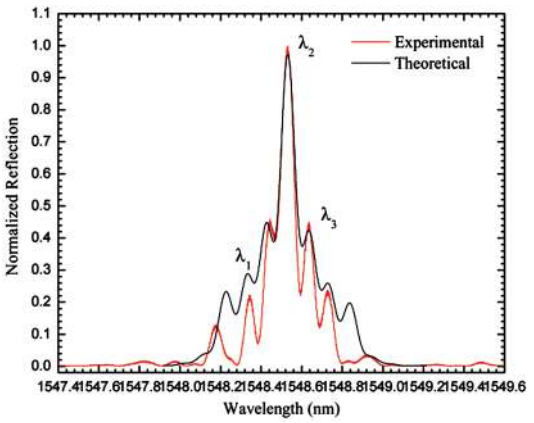

(c)

Figure 5. Reflection spectrum of: (a) FBG with an abrupt taper, (b) FBG with two abrupt tapers, and (c) FBG with three abrupt tapers.

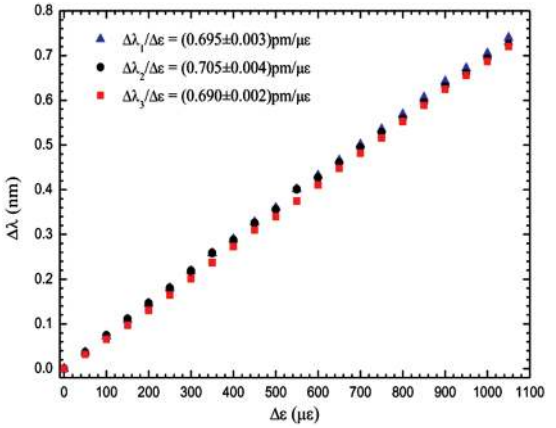

(a)

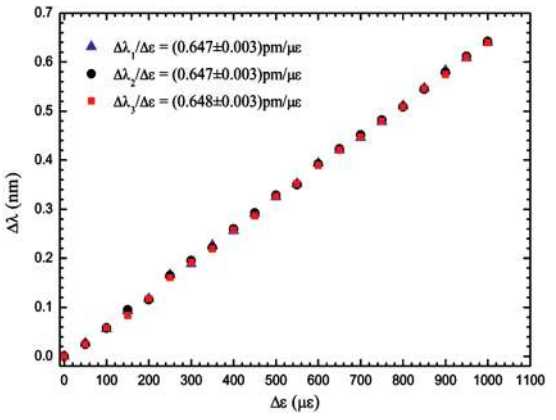

(b)

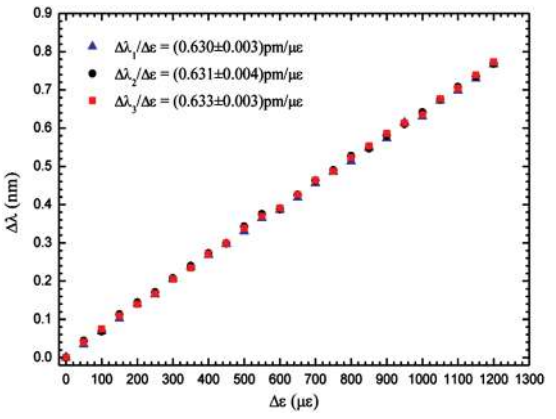

(c)

Figure 6. Wavelength shift versus applied strain of the peaks identified as λ_1, λ_2, and λ_3 in Figure 5 for: (a) TFP_1, (b) TFP_2, and (c) TFP_3.

Table 1
Strain coefficients of the TFP structures

	$\Delta\lambda/\Delta\varepsilon$ (pm/$\mu\varepsilon$)		
TFP structure	λ_1	λ_2	λ_3
TFP_1	0.695	0.705	0.690
TFP_2	0.647	0.647	0.648
TFP_3	0.630	0.631	0.633

is a slight decrease of the strain sensitivity values with the increase of the number of tapers in the grating.

It can also be observed that the obtained strain sensitivities are inferior to 1 pm/$\mu\varepsilon$ as obtained with a uniform Bragg grating. Since tapers have reduced fiber diameters, stress is higher is these regions when compared to the unperturbed FBG sections.

In Figure 5, the spectral envelope shift induced by strain is associated with the regions of the Bragg grating not affected by the taper fabrication. It is found that this envelope moves slower with applied strain than the interferometric fringes (wavelength peaks). This turns out from the observation of the peak power changes shown in Figure 7 (the peak powers associated with λ_1 and λ_3 are normalized to that identified λ_2, which is attributed a unitary value). The applied strain increases nL, but in order to keep the 2π phase difference between the reflected waves, the wavelength must also increase. By the envelope effect, the spectral peak associated with λ_1 increases and the spectral peak associated to λ_3 decreases. However, the envelope shifts as well. If the fringes and the envelope had a synchronous movement, then no peak power variations would be observed. The reason that λ_1 increases and λ_3 decreases must be that the fringes move faster than the envelope. Regardless, its continuous presence is a clear indication of the stated envelope displacement with strain. Indeed, in the case of TFP_1, 1,000 $\mu\varepsilon$ corresponds to a wavelength shift of 0.7 nm, which is much higher than the FWHM of the envelope ($\sim$0.2 nm). Therefore, if the envelope did not move, the referenced fringes would move out of it and soon would not be visible. This differential spectral displacement, and consequent differential strain sensitivity of the Fabry-Pérot and Bragg grating, is explained by the fact that the applied strain appears more in the taper regions due to the fiber reduced diameter in these regions and less in the unperturbed fiber sections, which are those where the Bragg grating refractive index modulation remains.

In the case of TFP_2 and TFP_3, results similar to those obtained for TFP_1 can be observed: the spectral peak associated to λ_1 increases, and the spectral peak associated to λ_3 decreases. However, a linear response is found that is not observed in TFP_1. This might be associated to different locations of the optical peaks relative to the envelope, or due to the presence of broad spectral envelopes that result from the length reduction of the Bragg grating sections with the increase of the number of tapers in the structure.

Figure 8 shows the wavelength variation of the spectral peaks of the TFP structures as a function of temperature. It can be observed that the obtained sensitivities are of the order of 10 pm/°C, similar to what can be found with a uniform Bragg grating operating at 1,550 nm (the wavelength shift of the peak identified as λ_1 in Figure 5a—single TFP structure—is not given due to its residual amplitude). Since the devices undergo

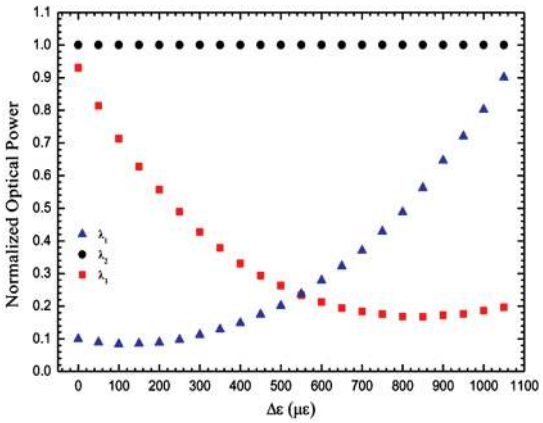

(a)

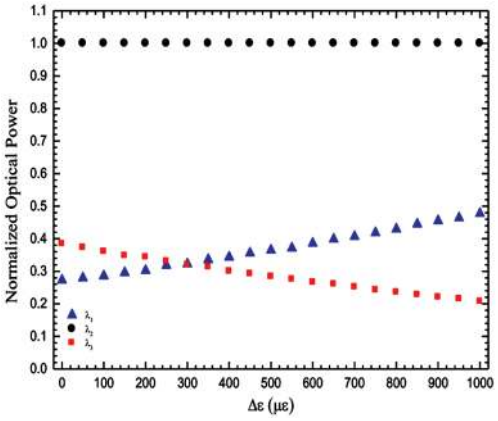

(b)

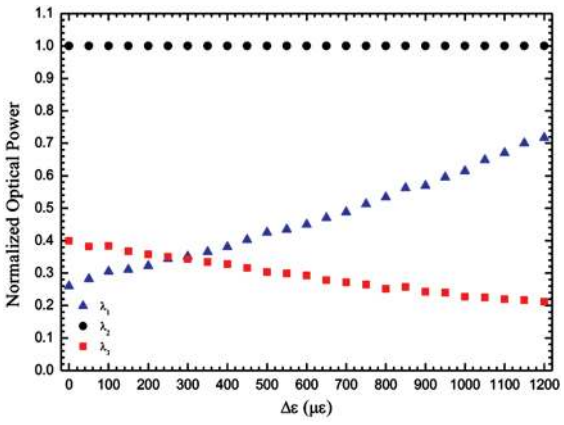

(c)

Figure 7. Amplitude of the peaks identified as λ_1 and λ_3 in Figure 5 normalized to the λ_2 peak (which is attributed the unitary value) versus applied strain for: (a) TFP_1, (b) TFP_2, and (c) TFP_3.

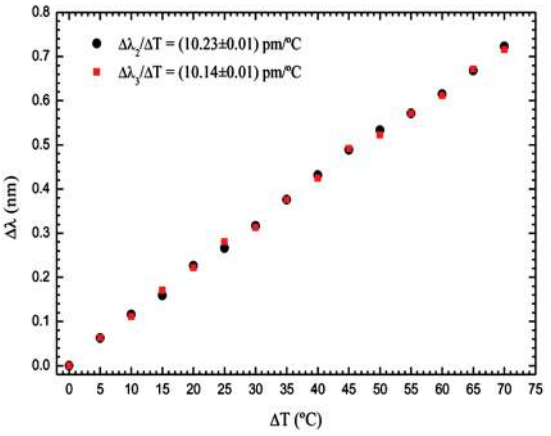

(a)

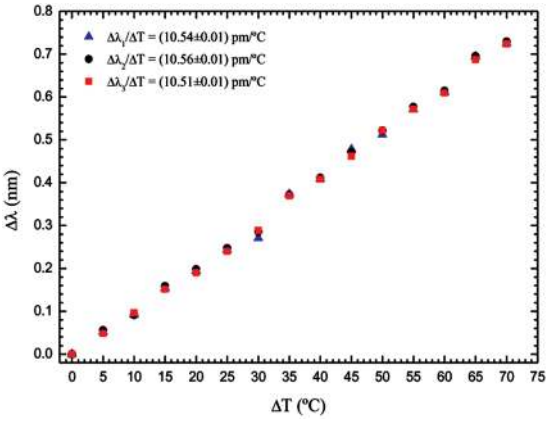

(b)

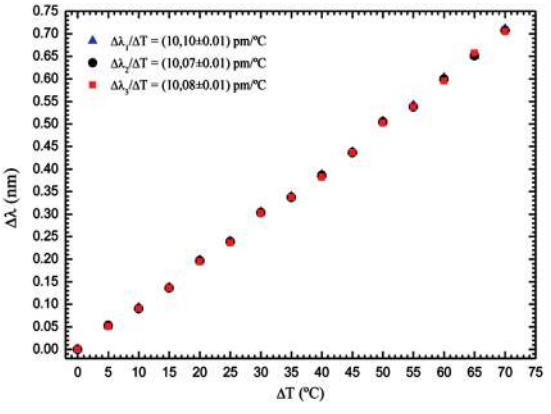

(c)

Figure 8. Wavelength shift versus temperature variation of the peaks identified as λ_1, λ_2, and λ_3 in Figure 5 for: (a) TFP_1, (b) TFP_2, and (c) TFP_3.

no geometric change when submitted to temperature variations, only the variation of the thermo-optic effect is observed.

It was also observed that the amplitude of the spectral peaks does not change with temperature. This happens because, in the case of temperature variation, the envelope of the spectral response of these sensing structures moves synchronously with the internal wavelength peaks (interferometric fringes). This can be confirmed through a simple analysis of the relevant equations. Using the grating Bragg condition ($\lambda_B = 2n_{eff}\Lambda$) and the interferometric phase term ($\phi = 4\pi nL/\lambda$), the following relations are obtained:

$$\lambda_B = 2n\Lambda \Rightarrow \partial\lambda_B = \lambda_B \frac{\partial n}{n},$$

$$\begin{cases} \partial\phi = \dfrac{4\pi L}{\lambda}\partial n \\ \partial\phi = -\dfrac{4\pi nL}{\lambda^2}\partial\lambda \end{cases} \Rightarrow \partial\lambda = \lambda\frac{\partial n}{n}.$$

These equations show that the displacement of the envelope and the displacement of the internal interferometric fringes as a function of the refractive index variation are the same.

One consequence of this result is that the determination of the amplitude of certain peaks of the spectral transfer function of these structures permits temperature independent strain measurement, a feature that is not exhibited by many sensing heads oriented to measurement of strain. Also, power referencing is easily accessible with these sensing configurations. Additionally, combining the monitoring of the amplitude of those peaks with any of their wavelength shifts makes possible the simultaneous measurement of strain and temperature, which adds extra flexibility to the utilization of these TFP structures.

The results presented addressed the sensing characteristics of the structures formed by inducing a fused taper in an FBG. As indicated before, another possibility is feasible, namely the fabrication of an FBG in a tapered fiber ($TFBG_2$).

Figure 9 shows the spectral responses of three tapered FBG devices that were obtained experimentally. Each grating has ~10 mm length, and the fused tapers are ~400 μm. Figures 9a, 9b, and 9c are relative to a Bragg grating written over one fiber taper ($TFBG_{2a}$), over two fiber tapers ($TFBG_{2b}$), and over three fiber tapers ($TFBG_{2c}$), respectively. The spectral response of these devices exhibits a channeled structure, an indication that there are cavity-like interferometric effects. They may arise from the taper-induced modulation of the effective refractive index of the guided mode, from different amplitudes of the Bragg grating refractive index modulation in the fiber regions that undertook the tapering process, or both.

The behavior of these TFBG devices in the situation of variable applied strain and temperature was also experimentally studied. For the case of strain, the obtained results relative to the spectral shifts of the fringes are shown in Figure 10. It can be observed that the obtained sensitivities are inferior to those associated with a uniform Bragg grating. Also, as shown in Table 2, the increase of the number of taper sections along each Bragg grating structure does not significantly affect the wavelength sensitivity to the strain of the optical peaks, which is residually lower when compared with the values obtained for the TFP devices (Table 1).

Following an argument similar to the one developed in the context of the TFP devices, it was observed that the envelope of each $TFBG_2$ structure moves slower than the corresponding spectral internal peaks.

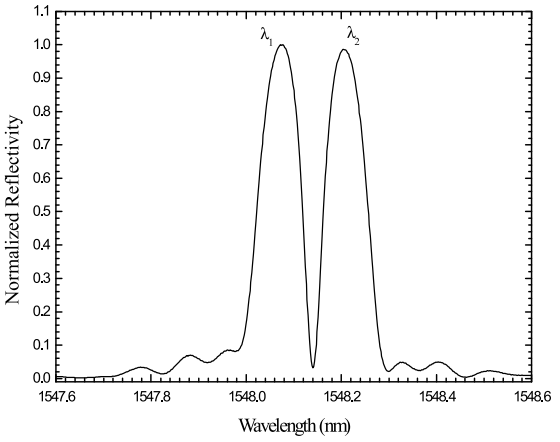

(a)

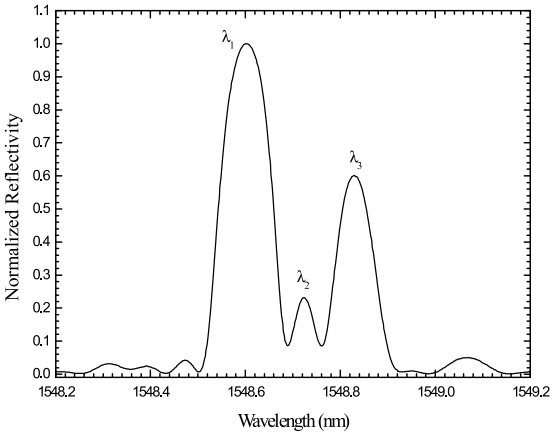

(b)

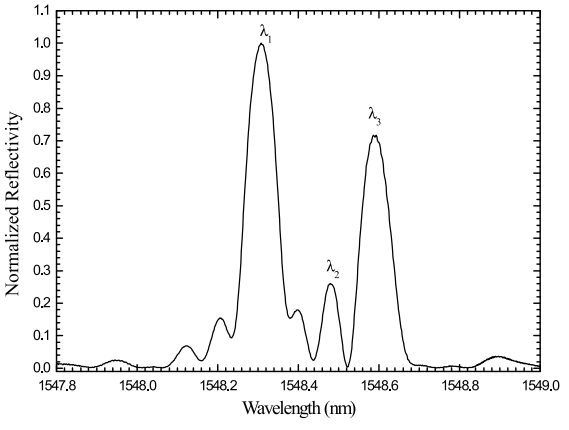

(c)

Figure 9. Reflection spectrum of: (a) Bragg grating written over a short fiber taper ($TFBG_{2a}$), (b) Bragg grating written over two short fiber tapers equally spaced ($TFBG_{2b}$), and (c) Bragg grating written over three short fiber tapers equally spaced ($TFBG_{2c}$).

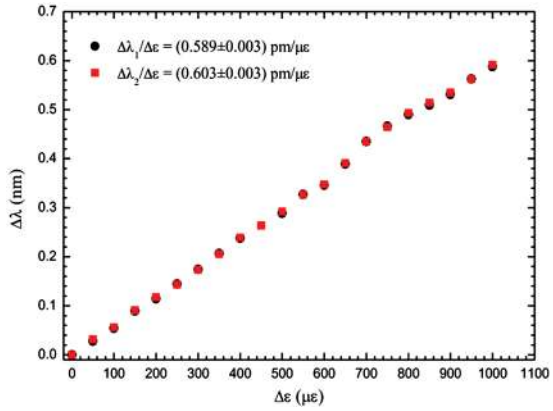

(a)

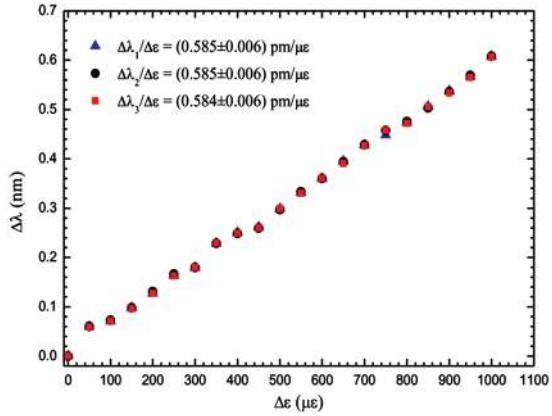

(b)

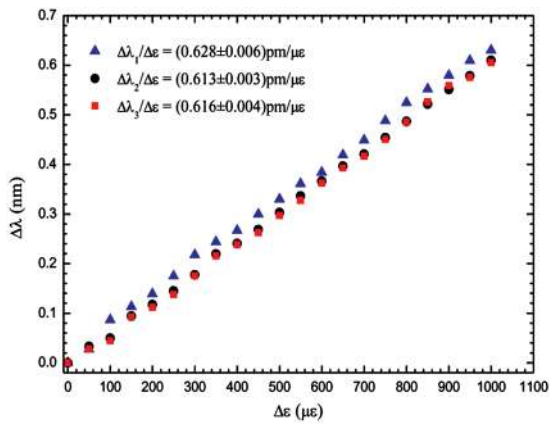

(c)

Figure 10. Wavelength shift versus applied strain of the peaks identified as λ_1, λ_2, and λ_3 in Figure 9 for: (a) $TFBG_{2a}$, (b) $TFBG_{2b}$, and (c) $TFBG_{2c}$.

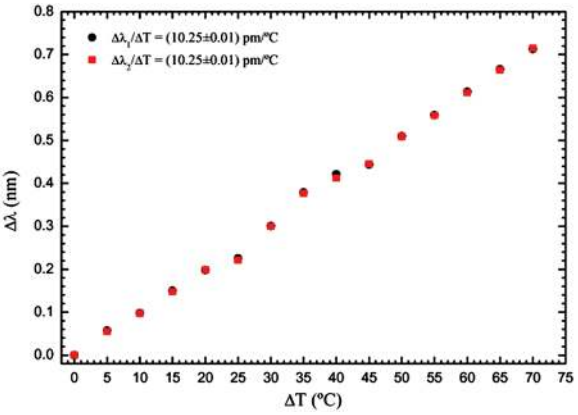

(a)

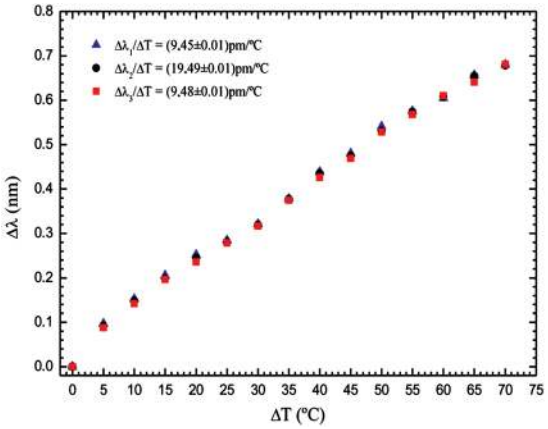

(b)

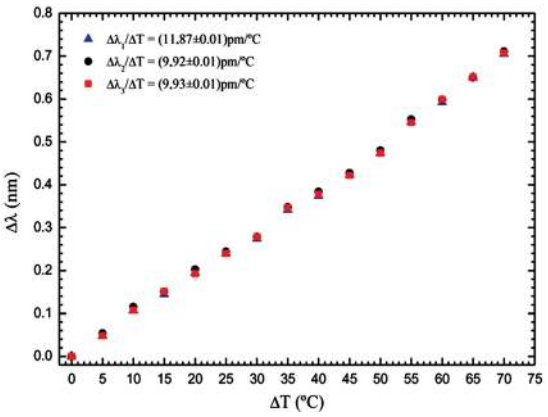

(c)

Figure 11. Wavelength shift versus temperature variation of the peaks identified as λ_1, λ_2, and λ_3 in Figure 9 for: (a) $TFBG_{2a}$, (b) $TFBG_{2b}$, and (c) $TFBG_{2c}$.

Table 2
Strain coefficients of the TFP structures

	$\Delta\lambda/\Delta\varepsilon$ (pm/$\mu\varepsilon$)		
$TFBG_2$ structure	λ_1	λ_2	λ_3
$TFBG_{2a}$	—	0.589	0.603
$TFBG_{2b}$	0.585	0.585	0.584
$TFBG_{2c}$	0.628	0.613	0.616

Figure 11 shows the wavelength variation of the spectral peaks of the $TFBG_2$ devices as a function of temperature. It can be observed that the obtained sensitivities are similar to those associated with a uniform Bragg grating. In this case, the envelope of the spectral responses moves synchronously with the corresponding peaks. Therefore, the determination of the amplitude of certain peaks of the spectral transfer function of these devices also allows temperature independent strain measurement.

5. Conclusions

This work has reported the analysis of FBG structures with abruptly fused tapers. Two devices were studied—one based on tapers fabricated on an FBG length, the other on an FBG written over fused tapers. The first device presents Fabry-Perot type characteristics, since the taper fabrication process destroys the spatial integrity of the grating, smaller length gratings appear that perform as cavity mirrors. Concerning the second device, the taper (tapers) is fabricated first and after hydrogenization, an FBG is written over the structure, resulting into configurations that exhibit also Fabry-Pérot like behavior. The properties of these devices for strain and temperature sensing were investigated, resulting in positive indications of their potential to perform simultaneous measurement of these parameters.

References

1. Gonthier, F., Lacroix, S., Daxhelet, X., Black, R. J., and Bures, J. 1989. Broadband all-fiber filters for wavelength-division-multiplexing application. *Applied Physics Letters* 54(14):1290–1292.
2. Tub, A. J. C., Payne, F. P., Millington, R. B., and Lowe, C. R. 1997. Single-mode optical fibre surface plasma wave chemical sensor. *Sensing Actuators B* 41(1–3):71–79.
3. Pendock, G. J., MacKenzie, H. S., and Payne, F. P. 1993. Dye lasers using tapered optical fibers. *Applied Optics* 32(27):5236–5242.
4. Kawasaki, B. S., Hill, K. O., and Lamont, R. G. 1981. Biconical-taper single mode fiber coupler. *Optics. Letters* 6(7):327–328.
5. Birks, T. A. 1989. Twist-induced tuning in tapered fiber couplers. *Applied Optics* 28(19):4226–4233.
6. Caspar, C., and Bachus, E. J. 1989. Fibre-optic micro-ring-resonator with 2 mm diameter. *Electronics Letters* 25:1506–1508.
7. Bobb, L. C., Shankar, P. M., and Krumboltz, H. D. 1990. Bending effects in biconically tapered single-mode fibers. *Journal of Lightwave Technology* 8(7):1084–1090.
8. Jedrzejewski, K. P., Martinez, F., Minelly, J. D., Hussey, C. D., and Payne, F. P. 1986. Tapered-beam expander for single-mode optical-fibre gap devices. *Electronics Letters* 22:105–106.

9. Putnam, M. A., Williams, G. M., and Friebele, E. J. 1995. Fabrication of tapered strain-gradient chirped fibre Bragg gratings. *Electronics Letters* 31(4):309–310.
10. Dong, L., Cruz, J. L., Reekie, L., and Tucknott, J. A. 1995. Fabrication of chirped fibre gratings using etched tapers. *Electronics Letters* 31(11):908–909.
11. Wei, Z., Li, H., Zheng, W., and Zhang, Y. 2001. Fabrication of tunable nonlinearly chirped fiber gratings using fiber Bragg grating. *Optics Communications* 187:369–371.
12. Quetel, L., Rivoallan, L., Morvan, M., Monerie, M., Delevaque, E., Guilloux, J. Y., and Bayon, J. F. 1997. Chromatic dispersion compensation by apodised Bragg gratings within controlled tapered fibers. *Optical Fiber Technology* 3:267–271.
13. Kenny, R. P., Birks, T. A., and Pakley, K. P. 1991. Control of optical fibre taper shape. *Electronics Letters* 27(18):1654–1656.
14. Mora, J., Villatoro, J., Díez, A., Cruz, J. L., and Andrés, M. V. 2002. Tunable chirp in Bragg gratings written in tapered core fibers. *Optics Communications* 210:51–55.
15. Du, W., Tao, X., and Tam, H. 1999. Temperature independent strain measurement with a fiber grating tapered cavity sensor. *IEEE Photonics Technology Letters* 11(5):596–598.
16. Frazão, O., Melo, M., Marques, P. V. S., and Santos, J. L. 2005. Chirped Bragg grating fabricated in fused fibre taper for strain-temperature discrimination. *Measurement Science and Technology* 16:984–988.
17. Frazão, O., Silva, S. F. O., Guerreiro, A., Santos, J. L., Ferreira, L. A., and Araújo, F. M. 2007. Strain sensitivity control of fiber Bragg grating structures with fused tapers. *Applied Optics* 46(36):8579–8582.
18. Stewart, W. J., and Love, J. D. 1985. Design limitation on tapers and couplers in single mode fibres. *11th European Conference on Optical Communication*, Venice, Italy, October 1–4, pp. 559–562.
19. Love, J. D., and Henry, W. M. 1986. Quantifying loss minimisation in single-mode fibre tapers. *Electronics Letters* 22:912–914.
20. Bures, J., Lacroix, S., and Lapierre, J. 1983. Analysis of a bidirectional coupler using a fusion single mode fibre [Analyse d'un coupleur bidirectionnel a fibres optiques monomodes fusionnees]. *Applied Optics* 22(12):1918–1922.
21. Burns, W. K., Abebe, M., and Villarruel, C. A. 1985. Parabolic model for shape of fiber taper. *Applied Optics* 24(17):2753–2755.
22. Birks, T. A., and Li, Y. W. 1992. The shape of fiber tapers. *Journal of Lightwave Technology* 10(4):432–438.
23. Love, J. D., Henry, W. M., Stewart, W. J., Black, R. J., Lacroix, S., and Gonthier, F. 1991. Tapered single-mode fibres and devices. Part 1: Adiabaticity criteria. *Proc. IEEE* 138(5):343–353.
24. Nunes, F. D., Melo, C. A. S., and Filho, H. F. S. 1996. Theoretical study of coaxial fibers. *Applied Optics* 35(3):388–399.
25. Adams, M. J. 1981. *An Introduction to Optical Waveguides*. New York: Wiley.
26. Melloni, A., Floridi, M., Morichetti, F., and Martinelli, M. 2003. Equivalent circuit of Bragg gratings and its application to Fabry-Pérot cavities. *Journal of the Optical Society of America A* 20(2):273–281.

Biographies

S. F. O. Silva received her Licenciatura in applied physics (optics and electronics) and her M.Sc. in optoelectronics and lasers from the University of Porto, Porto, Portugal, in 2004 and 2007, respectively, and is currently working toward her Ph.D. in physics at the University of Porto, Porto, Portugal. She is presently with INESC Porto in the Optoelectronics and Electronic Systems Unit. She has published 10 papers in international journals and more than 20 papers in national and international conferences. Her research interests include fiber-optic sensing, Bragg grating technology and biosensing. She is a member of EOS.

L. A. Ferreira graduated in 1991 in applied physics (optics and electronics) and in 1995 received his M.Sc. in optoelectronics and lasers (white-light interferometry and signal processing in optical fiber sensors), both from the University of Porto, Porto, Portugal. He received his Ph.D. in physics from the University of Porto in 2000 in interrogation of fiber-optic Bragg grating sensors, after developing part of his research work in fiber-optic sensing in the Physics Department, University of North Carolina, Charlotte. He is currently an engineering manager at FiberSensing, an INESC Porto spin-off company that he co-founded, which develops, manufactures, and installs advanced monitoring systems based on fiber-optic sensing technology and addresses markets such as structural health monitoring in civil and geotechnical engineering, aerospace, and energy production and distribution. He is also a senior researcher at the Optoelectronics and Electronic Systems Unit of INESC Porto, where he develops his main R&D activity in the areas of fiber-optic sensing and optical communications. He is author/co-author of more than 100 international communications, papers, and patents in the fields of fiber-optic sensing and fiber-optic communications.

F. M. Araújo graduated in 1993 in applied physics (optics and electronics) from the University of Porto, Portugal. He received his Ph.D. in physics from the University of Porto in 2000 (fiber Bragg gratings). He is a co-founder of and the Product Development Director with FiberSensing, an INESC Porto spin-off company, developing fiber-optic sensors and systems for different markets, such as structural health monitoring. He is also a senior researcher with the Optoelectronics and Electronic Systems Unit of INESC Porto. His main activity research is related with optical communications and fiber-optic sensing. Previous positions included leadership of the Fiber Optic Technologies Unit at MultiWave Networks Portugal (a company developing subsystems for fiber-optic communications), anassistant professor in the Physics Department of the University of Porto (Faculty of Sciences), and a senior researcher at the Optoelectronics and Electronic Systems Unit of INESC Porto, where he developed research in the area of fiber-optic technologies from 1993 to 2001. He is author/coauthor of more than 100 international communications, papers, and patents in the fields of fiber-optic sensing and fiber-optic communications.

J. L. Santos graduated in applied physics (optics and electronics) from the University of Porto (1983). He receive his Ph.D. from the same university (1993, "Multiplexing and Signal Processing in Fibre Optic Sensors"; research performed partially at the Physics Department of University of Canterbury, Kent, UK). His main research interests are in the optical fiber sensing field and in optical fiber technology. He is an associate professor in the Physics Department of the University of Porto, and he is also the manager of INESC Porto Optoelectronics and Electronics Systems Unit. He is member of OSA, SPIE, and PLANETARY SOCIETY.

O. Frazão graduated in physics engineering (optoelectronics and electronics) from the University of Aveiro, Aveiro, Portugal. He received his Ph.D. from the University of Porto, Porto, Portugal, in optical fiber sensors based on interferometry and non-linear effect. From 1997 to 1998, he was with the Institute of Telecommunications, Aveiro. He is now a senior researcher at Optoelectronics and Electronic Systems Unit, INESC Porto. His research interests include optical fiber sensors and optical communications. He has published in 98 peer-reviewed journals and over 220 papers in international and national conference proceedings and has authored 7 patents. He is a member of the OSA and SPIE.